Topological Hall effect in three-dimensional centrosymmetric magnetic skyrmion crystals

Andrei Zadorozhnyi and Yuri Dahnovsky

Phys. Rev. B **107**, 054436 — Published 24 February 2023

DOI: 10.1103/PhysRevB.107.054436

Topological Hall effect in 3D centrosymmetric skyrmion magnetic crystals

Andrei Zadorozhnyi and Yuri Dahnovsky

Department of Physics and Astronomy/3905

1000 E. University Avenue

University of Wyoming

*Laramie, WY 82071**

(Dated: February 14, 2023)

Abstract

Centrosymmetric skyrmions attract much attention from the research community because of their small sizes and high concentrations. These features can be useful for applications. Such skyrmions are originated due to the RKKY and Kondo interactions rather than the DMI. We study a topological Hall effect in such systems using the Boltzmann equation for a nonequilibrium distribution function. For the relaxation, we choose the electron-acoustic phonon and electron-skyrmion interactions. We find that the topological Hall resistivity exhibits the nonlinear behavior depending on chemical potential. Because of noncubic lattice symmetry, we investigate the dependence of the resistivity tensor components along with the x-direction (parallel to an applied electric field), ρ_{xx}, ρ_{zz} (the component along with the z-axis), and ρ_{xy} (a topological Hall component) with respect to the effective mass ratio, m_z/m_x. We assume that the skyrmions are spaced on the (xy)-plane and stretched out along with the z-direction. The temperature dependence of the resistivity tensor reveals the monotonic growth for all components. There is some concern in the interpretation of experiments. Sometimes it can be very difficult to measure the topological Hall resistivity. Indeed, we find that ρ_{xy} is one-two orders of magnitude less than ρ_{xx} and ρ_{zz}. Additionally, there is another important factor, which complicates the problem. The z-axis and an applied electric field are not exactly perpendicular because of experimental conditions. Thus, the perpendicular to the electric field resistivity contains a linear combination of ρ_{xy} and $|\rho_{xx} - \rho_{zz}|$. To determine ρ_{xy} from an experiment, we propose the experimental setup how to measure the topological Hall effect and provide the equations that allow us to determine ρ_{xy}.

I. INTRODUCTION

Magnetic skyrmion crystals have been of interest of the reach community for more than three decades.[1,2] Such magnetic spin-textures are usually stabilized by the Dzyaloshinski-Moria interaction (DMI) and take place in chiral magnets such as MnSi, $Fe_{1-x}Co_xSi$, FeGe, Cu_2OSO_2.[3–7] They are characterized by a topological charge, which is a nonzero integer. There have been recently discovered magnetic material with a nonzero topological charge in centrosymmetric 3D crystals where we do not expect any DMI at all. These materials are $BaFe_{1-x-0.05}Sc_xMg_{0.05}O_{19}$, $La_{2-2x}Sc_{1+2x}Mn_2O_7$, Gd_2PdSi_3,[8,9] $Gd_3Ru_4Al_{12}$,[10] $GdRu_2Si_2$,[11,12] Mn_4Ga_2Sn,[13] and $EuAl_4$,[14,15] Centrosymmetric skyrmion textures are stabilized by exchange coupling and spin dipolar interactions.[14] There are two mechanisms, which can generate skyrmions: (a) the Ruderman-Kittel-Kasuya-Yosida (RKKY) and(b) Kondo interactions.[16–19] It is also important to note that such skyrmions are usually small, with the diameter about 5 nm, which is about ten times smaller than conventional skyrmions that are originated from DMI. Such small skyrmions are packed closely together in 3D $EuAl_4$ crystals with the separation distance of 3.5 nm.[14] Small size skyrmion materials can be very useful for applications in modern computers because their large memory density. Another very important property that should be mentioned is that such small size skyrmions can be very efficient as electron (or hole) scattering centers.

In this research we theoretically and numerically investigate charge transport properties in centrosymmetric 3D crystals and study how direct and topological Hall resistivities depend on chemical potential, μ, and temperature. The methodology for the calculation of different components in electric current is based on the Boltzmann equation for a noneqiuilibrium distribution function.[20,21] To find it, we consider the two scattering mechanisms: (a) the electron-acoustic phonon and (b) electron-skyrmion interactions.[22–24] We include the electron-phonon interaction for the following reasons: (a) the interaction between electrons and phonons always takes place, (b) if the electron-phonon interaction is excluded, the σ_{zz} component goes to infinity, and (c) it provides the additional temperature dependence in electric current. The temperature dependence of electric current comes from two sources: (a) the Fermi distribution function and (b) the Bose-Einstein phonon distribution function. There can be another approach where the magnetic and electric emergent fields can substitute the interaction between electrons and skyrmions.[21,25–28] Using this approach, *MnSi*

skyrmion phase was studied in Refs.[25,26,29]. The emergent electric field decreases the topological Hall current. Such a current drop is associated with skyrmion motion. The general theory and experimental observation of skyrmion motion without disorder was reported in Refs.[30,31], and with disordered magnetic skyrmions in Refs.[32,33] . It was also found that there is a threshold (pinning) current, j_{pin}, below which skyrmions do not move. In this work we assume that the currents are low and the skyrmions are static. The topological Hall effect in a skyrmion lattice in the Kubo approach was investigated in Refs.[34,35]. In this research we do not include the interaction between the skyrmions, i. e., we consider an ideal skyrmion gas rather than skyrmion crystal or liquid. In Ref.[36] the authors used the nonequilibrium Keldysh function technique to find the chiral Hall effect. The results may differ for lattice and for an ideal gas, but we expect the similar dependencies.There is an additional problem, which experimentalist can encounter in the detection of ρ_{xy} topological Hall resistivity. As we will show below, the topological Hall resistivity, ρ_{xy}, is less by one-two orders of magnitude than the difference between ρ_{xx} and ρ_{zz}. In this case, it can be very hard to detect ρ_{xy} because the values of ρ_{xx} and ρ_{zz} can dominate, especially if the current direction is not collinear with crystal x- or y- axes. Furthermore, we also investigate temperature and mass ratio dependences of a topological Hall and direct resistivities.

II. CHARGE TRANSPORT

In this section we present the methodology for the charge transport calculations. In particular, we study a 3×3 resistivity tensor, $\hat{\rho}$. The tensor component ρ_{xy} describes a topological Hall effect. The charge carriers, electrons or holes, scatter by both acoustic phonons and skyrmions.

A. Boltzmann equation

For the transport calculations we use the Boltzmann equation with the relaxation rate due to both electron-phonon and electron-skyrmion interactions in an ideal skyrmion gas:

$$\frac{\partial f_0}{\partial \varepsilon} e\boldsymbol{E} \cdot \boldsymbol{v}^{\nu} = \sum_{\nu'} \sum_{\boldsymbol{k}'} \left(W^{\nu\nu'}_{\boldsymbol{k}\boldsymbol{k}'} f_1^{\nu'}(\boldsymbol{k}') - W^{\nu'\nu}_{\boldsymbol{k}'\boldsymbol{k}} f_1^{\nu}(\boldsymbol{k}) \right), \tag{1}$$

where f_0 is the equilibrium Fermi distribution function, f_1 is the nonequilibrium part of the total distribution function, $\boldsymbol{E}$ is an applied electric field, and $\boldsymbol{v}$ is an electron velocity. There are two contributions in the total transition rates: $W^{\nu\nu'}_{\boldsymbol{k}\boldsymbol{k}'} = W^{\nu\nu'}_{(ph)\boldsymbol{k}\boldsymbol{k}'} + W^{\nu\nu'}_{(sk)\boldsymbol{k}\boldsymbol{k}'}$. The transition rates due to phonons, $W^{\nu\nu'}_{(ph)\boldsymbol{k}\boldsymbol{k}'}$, are calculated in the first Born approximation:

$$W^{\nu\nu'}_{(ph)\boldsymbol{k}\boldsymbol{k}'} = (2\pi/\hbar)\left|\left\langle \boldsymbol{k}', \nu', N'_{\boldsymbol{q}j}\right| \Delta V_{ph} \left|\boldsymbol{k}, \nu, N_{\boldsymbol{q}j}\right\rangle\right|^2 \delta(\varepsilon_\nu(\boldsymbol{k}) - \varepsilon_{\nu'}(\boldsymbol{k}')). \tag{2}$$

Here ΔV_{ph} is perturbation energy due to the $el-ph$ interaction. Then, the electron-acoustic phonon transition rates can be presented as follows:[20]

$$\begin{aligned} W^{\nu\nu'}_{(ph)\boldsymbol{k}\boldsymbol{k}'} = {} & \frac{2\pi}{\hbar}\frac{1}{NM}\frac{\hbar N_{\boldsymbol{q}j}}{2\omega_{\boldsymbol{q}}}\left|K^{+}_{\nu\nu'}\right|^2 \delta(\varepsilon_\nu(\boldsymbol{k}) - \varepsilon_{\nu'}(\boldsymbol{k}'))\delta(\boldsymbol{k}' - \boldsymbol{k} - \boldsymbol{q}) \\ & + \frac{2\pi}{\hbar}\frac{1}{NM}\frac{\hbar\left(N_{-\boldsymbol{q}j}+1\right)}{2\omega_{-\boldsymbol{q}}}\left|K^{-}_{\nu\nu'}\right|^2 \delta(\varepsilon_\nu(\boldsymbol{k}) - \varepsilon_{\nu'}(\boldsymbol{k}'))\delta(\boldsymbol{k}' - \boldsymbol{k} + \boldsymbol{q}), \end{aligned} \tag{3}$$

where

$$K^{\pm}_{\nu\nu'} = \pm i\frac{\hbar^2}{2ma^2}\frac{2}{3}\left(\boldsymbol{q}\cdot\boldsymbol{e}_{\boldsymbol{q}j}\right)\delta_{\nu\nu'}. \tag{4}$$

Here M is the single atom mass, N is the number of atoms in the crystal, $\omega_{\pm\boldsymbol{q}}$ is the frequency of the phonon with the wavevector $\boldsymbol{q}$, m is the free electron mass, a is a lattice constant, $\boldsymbol{e}_{\boldsymbol{q}j}$ is the polarization vector of the phonon on the branch j, and $N_{\boldsymbol{q}j}$ is the population number of phonons determined from the Bose distribution function:

$$N_{\boldsymbol{q}j} = \frac{1}{e^{\frac{\varepsilon_{ph}}{k_B T}} - 1}. \tag{5}$$

Index ν denotes an energy band number ($\nu = 1, 2$).

The transition rates due to the skyrmions, $W^{\nu\nu'}_{(sk)\boldsymbol{k}\boldsymbol{k}'}$, are calculated using the following equation:[37–39]

$$W^{\nu\nu'}_{(sk)\boldsymbol{k}\boldsymbol{k}'} = \frac{2\pi}{\hbar} n_{sk}\left|T^{\nu\nu'}_{\boldsymbol{k}\boldsymbol{k}'}\right|^2 \delta(\varepsilon_\nu(\boldsymbol{k}) - \varepsilon_{\nu'}(\boldsymbol{k}')), \tag{6}$$

where n_{sk} is the density of the skyrmions and the transition matrix $T^{\nu\nu'}_{\boldsymbol{k}\boldsymbol{k}'}$ is found from the Lippmann-Schwinger integral equation:[39]

$$\hat{T} = \hat{V}_{sk} + \hat{V}_{sk}\hat{G}_0\hat{T}, \tag{7}$$

where $\hat{G}_0$ is the free electron retarded Green's function, and $\hat{V}_{sk}$ is the perturbation due to the presence of skyrmions given by the following matrix:[40]

$$\hat{V}_{sk}(\mathbf{r}) = -J\begin{pmatrix} \delta n_z(\mathbf{r}) & \delta n_x(\mathbf{r}) - i\delta n_y(\mathbf{r}) \\ \delta n_x(\mathbf{r}) + i\delta n_y(\mathbf{r}) & -\delta n_z(\mathbf{r}) \end{pmatrix}. \tag{8}$$

For the skyrmion magnetic moment distribution, we choose the following analytic form:[41]

$$\begin{aligned}
\delta n_z(r) &= \begin{cases} 4\left(\frac{r}{a}\right)^2 - 2, \ r \le a/2, \\ -4\left(1 - \frac{r}{a}\right)^2, \ a/2 < r \le a, \\ 0, \ r > a, \end{cases} \\
\delta n_x(\boldsymbol{r}) &= \sqrt{1 - (\delta n_z(r) + 1)^2}\cos\alpha, \\
\delta n_y(\boldsymbol{r}) &= \sqrt{1 - (\delta n_z(r) + 1)^2}\sin\alpha,
\end{aligned} \tag{9}$$

where a is a skyrmion radius, r and α are polar coordinates in a frame with the center of the skyrmion located at $r = 0$. The magnetic moment is constant with z. In three dimensions the skyrmion resembles a 2D skyrmion on each layer that replicates in z direction as shown in Fig. 1.

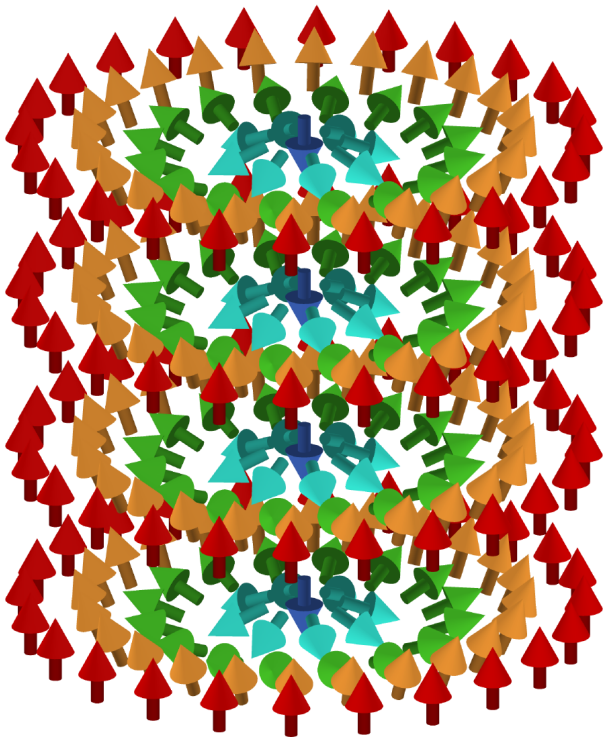

FIG. 1. 3D skyrmion.

As soon as the transition rates are found and the Boltzmann equation is solved for the first order correction the the equilibrium distribution function, we can determine the electric

current density:

$$j_i^\nu = \frac{e}{(2\pi)^3} \int f_1^\nu v_i^\nu d^3k, \tag{10}$$

where v_i^ν is a velocity projection ($i = x, y, z$) determined as $v_i^\nu = \partial\varepsilon^\nu(\boldsymbol{k})/\hbar\partial k_i$.

To solve the Boltzmann equation (1), we have written the original codes where the relaxation rates due to phonons are considered in the first Born approximation and relaxation rates due to skyrmions are found numerically from the Lippmann-Schwinger equation in all orders. For each $(\nu, \boldsymbol{k})$ and $(\nu', \boldsymbol{k}')$ at the energy surface, the transition rates have been determined and substituted into the integral Boltzmann equation, which has been numerically solved for f_1 in the piecewise constant approximation and then inserted into the expression for the current (see Eq. (10)). Once the relation between electric field and the current is found, we can find resistivity tensor defined as follows:

$$E_i = \sum_k \rho_{ik} j_k, \tag{11}$$

where $i, k = x, y, z$.

III. RESULTS AND DISCUSSIONS

In this research we study a resistivity tensor represented by the following matrix:

$$\hat{\rho} = \begin{pmatrix} \rho_{xx} & \rho_{xy} & 0 \\ -\rho_{xy} & \rho_{xx} & 0 \\ 0 & 0 & \rho_{zz} \end{pmatrix}. \tag{12}$$

In this matrix, $\rho_{xx} = \rho_{yy}$ and $\rho_{yx} = -\rho_{xy}$ because of the cylindrical symmetry of the material in xy-plane. Indeed, if an electric field is directed along with the x-axis, the Hall component is, for example, towards the positive y-direction. If we direct the electric field is along with the y axis in the same material, the electron will turn towards the negative x-direction. That is why $\rho_{yx} = -\rho_{xy}$. We note that the skyrmion potential is constant along with the z-axis and, therefore, does not scatter electrons in this direction. It means that there is only one scattering mechanism along with the z axis, the interaction with acoustic phonons, however, in the xy-plane, there are two electron scattering mechanisms, due to the $el - ph$

and electron-skyrmion interactions. Furthermore, using the same arguments we conclude that there are no ρ_{xz} and ρ_{yz} Hall components.

In centrosymmetric materials, as mentioned above, the crystal symmetry is noncubic. In this case, we have to study the transport properties of the electrons with non-symmetric energy band. In our model it means different effective masses:

$$\hat{H}_0 = \frac{\hbar^2 k_x^2}{2m_x} + \frac{\hbar^2 k_y^2}{2m_y} + \frac{\hbar^2 k_z^2}{2m_z}. \tag{13}$$

In this work we consider the crystal symmetry where $m_x = m_y$.

A. Chemical potential dependence

For calculations we consider $m_x = m_y = 0.5\ m_e$, where m_e is the free electron mass. $JS_0 = 0.05$ eV, the skyrmion diameter is 3.5 nm, and the density of the skyrmions is $1/6^2$ nm^{-2} corresponding to the 6 nm distance between the centers of the skyrmions. Thus, it is clear that the resistivity tensor components depend on the mass ratio, m_z/m_x. The results of the calculations for $m_z/m_x = 0.4, 1, 2$ are presented in Figs. 2, 3, and 4.

In Fig. 2a, 3a and 4a, ρ_{xx}- and ρ_{zz}-components are depicted depending on chemical potential, μ, for the mass ratios $m_z/m_x = 0.4, 1$, and 2, respectively. As expected, the resistivity drops because of the two factors: faster electrons participate in the current and the phase volume increases with μ. There is a very interesting interplay between the red (ρ_{xx}) and the blue (ρ_{zz}) curves. Indeed, as shown in Fig. 2a, ρ_{xx} is always greater than ρ_{zz} because the skyrmions do not scatter in the z-direction and, therefore, the resistivity is lower. Additionally, the effective mass m_z is lower than m_x and therefore, the electrons move faster in the z-directionn decreasing the resistivity. In the case of equal masses (Fig. 3a,) ρ_{xx} is still greater than ρ_{zz} because of the scattering due to the skyrmions. If $m_z/m_x = 2$ (see Fig. 4a) ρ_{zz} is greater than ρ_{xx} at low μ because of the slower electron motion in the z-direction. However, at larger μ, the phase space increases and we observe the curve crossing where ρ_{xx} becomes greater than ρ_{zz}. A peculiar feature can be found near the bottom of the upper energy band. In this case, ρ_{xx} exhibits a kink while the ρ_{zz} does not have it. Thus, we conclude that electron-skyrmion scattering is in charge of such a behavior. Indeed, if μ is slightly above the bottom of the upper band, the electrons from the lower one can be scattered by the skyrmions to the upper band where the velocities are small. Thus,

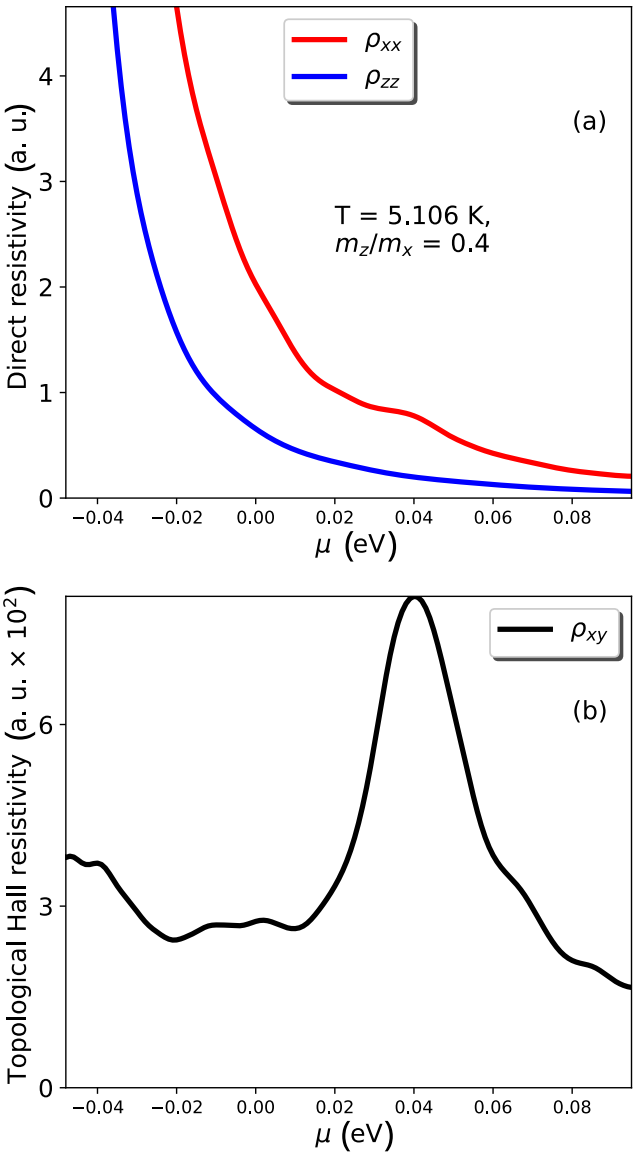

FIG. 2. Chemical potential dependence of the resistivity tensor components for $m_z/m_x = 0.4$ and $T = 5$ K. In (a) the red line stands for ρ_{xx}, the blue line stands for ρ_{zz}, and the black line in (b) represents ρ_{xy}.

the resistivity increases for the current along with the x-axis. Then, the resistivity drops because velocities become higher at larger μ.

The topological Hall component in resistivity only depends on the skyrmion scattering being independent of the z-direction. Even though, the shape of $\rho_{xy}(\mu)$ is almost independent

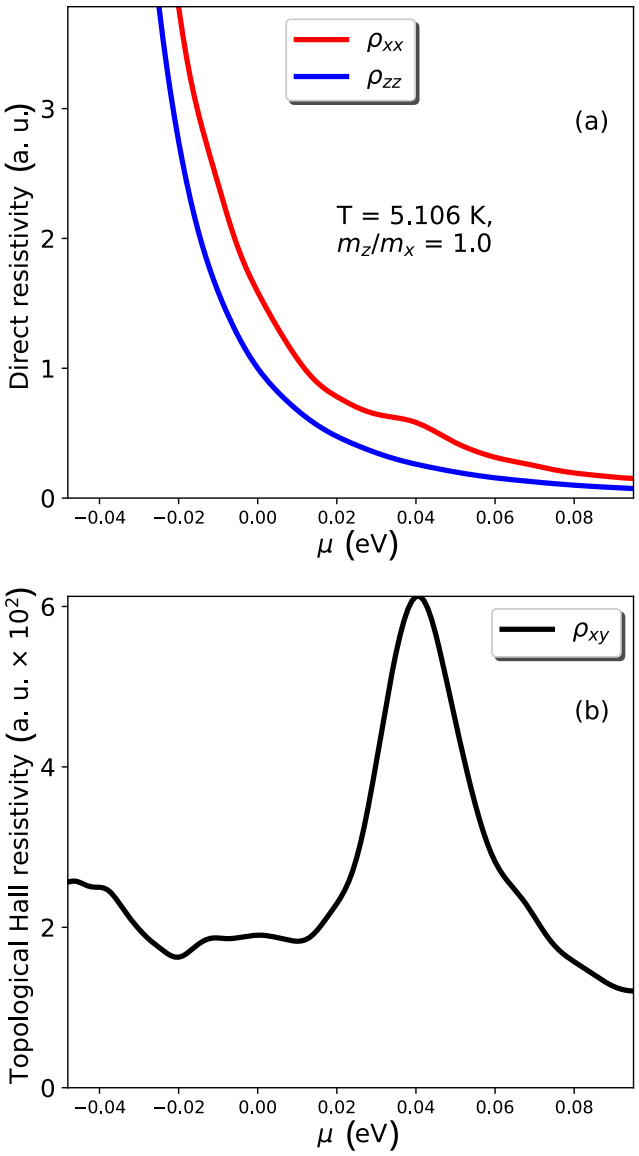

FIG. 3. Chemical potential dependence of the resistivity tensor components for $m_z/m_x = 1$ and $T = 5$ K. In (a) the red line stands for ρ_{xx}, the blue line stands for ρ_{zz}, and the black line in (b) stands for ρ_{xy}.

of the mass ratio, and the absolute values drop by twice from $m_z/m_x = 0.4$ to $m_z/m_x = 2$. In our calculations we keep m_x constant and change m_z. Such an m_z-dependence we explain by the increase of the phase volume with m_z, stretching out the k-space in the z-direction. The higher m_z, the higher the current in the xy-plane, and, therefore, the lower the resistivity.

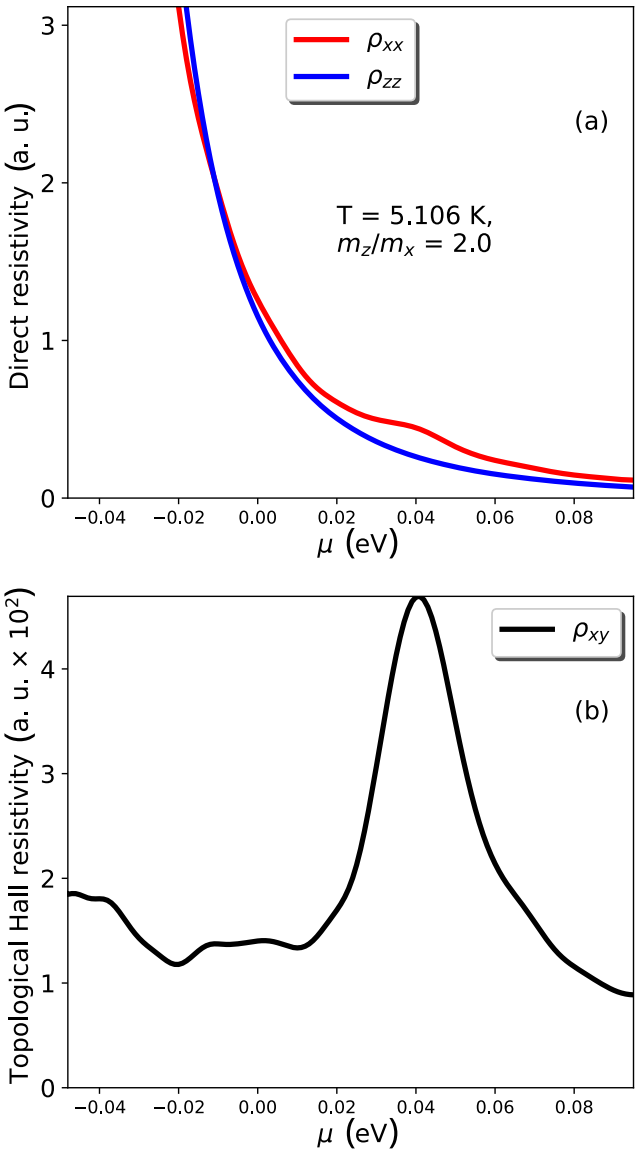

FIG. 4. Chemical potential dependence of the resistivity tensor components on for $m_z/m_x = 2$ and $T = 5$ K. In (a) the red line stands for ρ_{xx}, the blue line stands for ρ_{zz}, and the black line in (b) represents ρ_{xy}.

Such a picture is presented in Figs. 2b - 4b. The peak-dependence in ρ_{xy} in all three figures can be explained in a similar way as for the peak in ρ_{xx} shown in Figs. 2a - 4a. Indeed, if μ is close to the bottom of the upper energy band, the strong interband transitions take place where the fast electrons from the lower band become the slower electrons on the upper band

and, therefore, the resistivity increases. Then, the resistivity drops because of the higher velocities at the upper bands and also the larger phase volume.

B. Temperature dependence

The dependencies of ρ_{xx}, ρ_{zz} and ρ_{xy} on temperature for $m_z/m_x = 0.4, 1$, and 2 are presented in Figs. 5, 6, and 7. As expected, the resistivities ρ_{xx} and ρ_{zz} increase with temperature because of increase of the scattering due to the interaction between electrons and acoustic phonons. The most nontrivial behavior is for $m_z/m_x = 2$. In this case, we see the intersection of the red and blue curves in Fig. 7a. At lower temperatures the skyrmion scattering dominates and, therefore, $\rho_{xx} > \rho_{zz}$. With the increase of temperature, the electron-phonon interaction is more and more pronounced prevailing over the electron-skyrmion scattering. The curves are parallel if the effective masses are equal ($m_z = m_x$, see Fig. 6a). If m_z is greater than m_x, the resistivity ρ_{zz} becomes higher than ρ_{xx} in the temperature dependence. Thus, we observe the curve crossing.

The temperature dependence of topological Hall resistivity is less dramatic. It increases with temperature because of the more efficient electron-phonon scattering and the increase of the phase volume.

IV. PROPOSED EXPERIMENTAL SETUP TO OBSERVE TOPOLOGICAL HALL EFFECT

It is not easy to measure topological Hall resistivity ρ_{xy} because its value is one-two orders of magnitude lower than ρ_{xx} and ρ_{zz}. In addition, there is another important factor that cause problems in the experiment interpretation if the z-axis and an applied electric field are not perpendicular because of experimental conditions. To find electric resistivity components perpendicular to the electric field assuming the current is aligned with the new x''-axis, we should rotate the frame.

First, we rotate our system about the x-axis by the angle θ. The second rotation is about

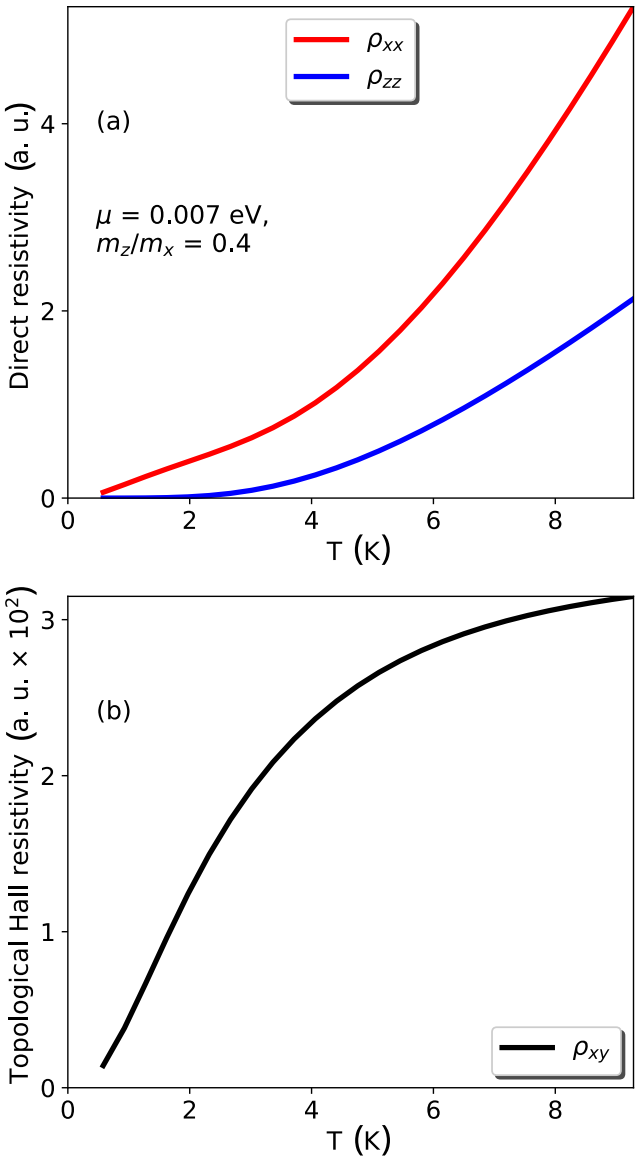

FIG. 5. Temperature dependence of the resistivity tensor components for $m_z/m_x = 0.4$ and $\mu = 0.07$ eV. In (a) the red line stands for ρ_{xx}, the blue line stands for ρ_{zz}, and the black line in (b) represents ρ_{xy}.

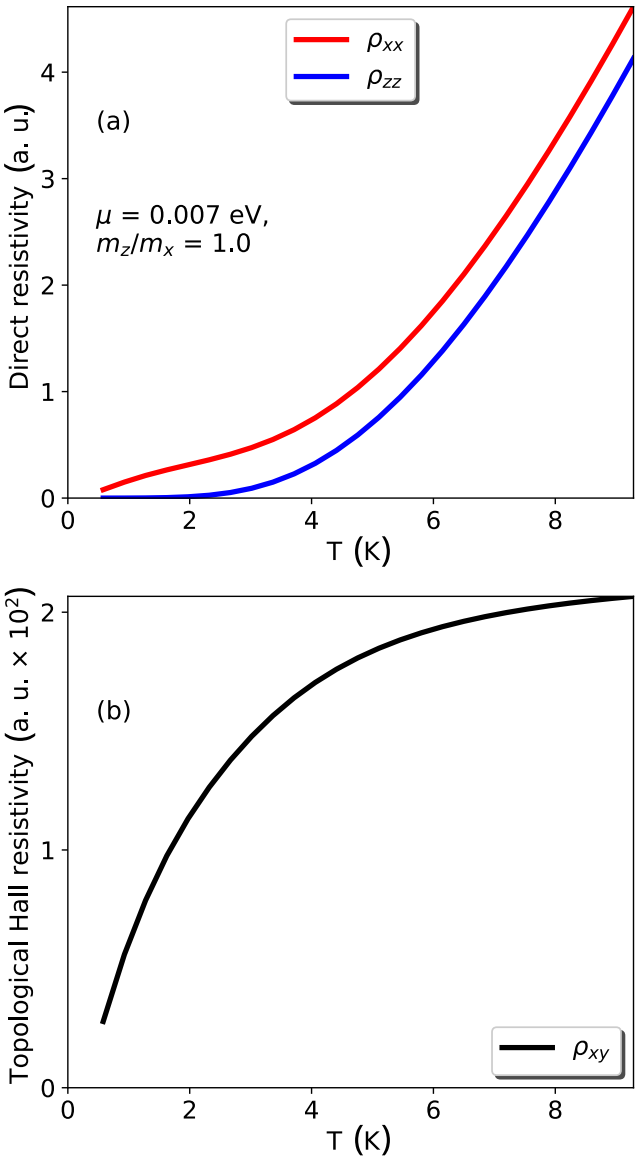

FIG. 6. Temperature dependence of the resistivity tensor components for $m_z/m_x = 1$ and $\mu = 0.07$ eV. In (a) the red line stands for ρ_{xx}, the blue line stands for ρ_{zz}, and the black line in (b) represents ρ_{xy}.

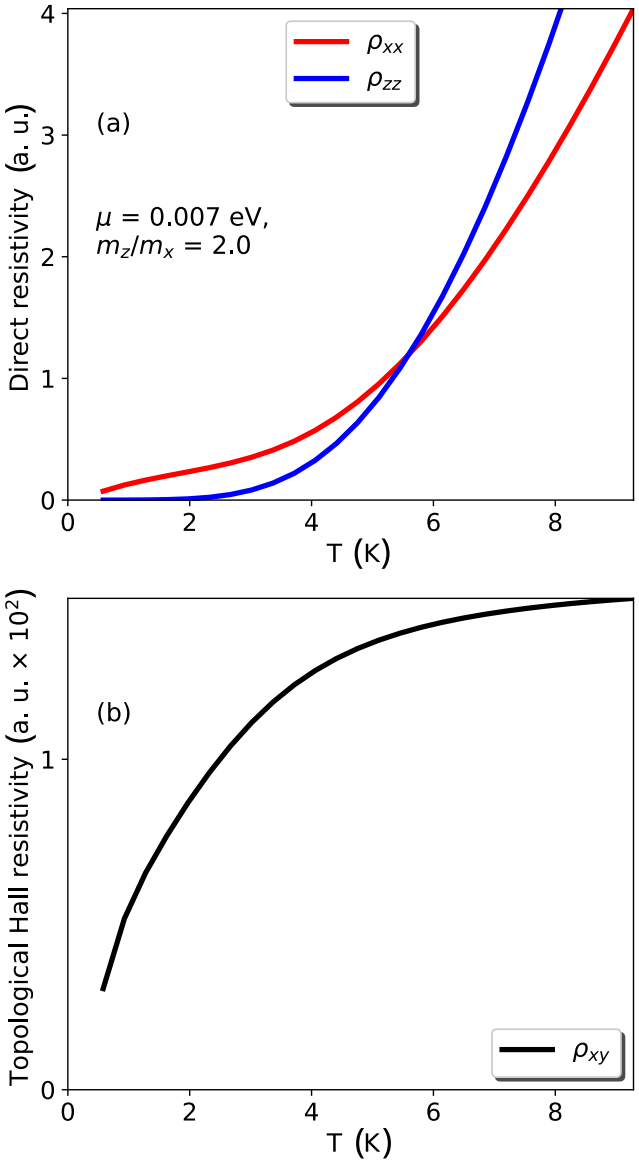

FIG. 7. Temperature dependence of the resistivity tensor components for $m_z/m_x = 2$ and $\mu = 0.07$ eV. In (a) the red line stands for ρ_{xx}, the blue line stands for ρ_{zz}, and the black line in (b) represents ρ_{xy}.

the new axis z' by the angle φ. The rotation matrix can be written as follows:

$$M = \begin{pmatrix} \cos\varphi & -\sin\varphi & 0 \\ \sin\varphi & \cos\varphi & 0 \\ 0 & 0 & 1 \end{pmatrix} \begin{pmatrix} 1 & 0 & 0 \\ 0 & \cos\theta & -\sin\theta \\ 0 & \sin\theta & \cos\theta \end{pmatrix} = \begin{pmatrix} \cos\varphi & -\sin\varphi\cos\theta & \sin\varphi\sin\theta \\ \sin\varphi & \cos\varphi\cos\theta & -\cos\varphi\sin\theta \\ 0 & \sin\theta & \cos\theta \end{pmatrix} \quad (14)$$

Because of the cumbersome expressions, we only write the first column of the new resistivity matrix ρ'':

$$\begin{aligned} \rho''_{xx} &= \rho_{xx} + \sin^2\varphi\sin^2\theta\left(\rho_{zz} - \rho_{xx}\right), \\ \rho''_{yx} &= -\cos\theta\rho_{xy} - \sin\varphi\cos\varphi\sin^2\theta\left(\rho_{zz} - \rho_{xx}\right), \\ \rho''_{zx} &= -\sin\theta\cos\varphi\rho_{xy} + \sin\varphi\sin\theta\cos\theta\left(\rho_{zz} - \rho_{xx}\right) \end{aligned} \quad (15)$$

If, for example, the current is directed along with the new x''-axis, the y''-component of the electric field would have two terms, the latter can be much larger by one-two orders of magnitude than the former. However, if an experimentalist knows the exact values of θ and φ, they will be able to determine ρ_{xy} from the system of linear algebraic equations (15). To find the true value of the Hall resistivity, we have to know the voltage in all three directions. To perform such measurements, we propose the following experimental setup shown in Fig. 8 allowing for the measurements of $V_{x''}$, $V_{y''}$, $V_{z''}$.

V. CONCLUSIONS

In this work we have considered the transport and topological Hall effect in materials with 3D centrosymmetric skyrmions. We have studied the direct and topological Hall resistivities depending on chemical potential (an electron concentration) and temperature. We have found that the topological Hall resistivity exhibits the nonlinear behavior and depends on the mass ratio m_z/m_x. The peaks in ρ_{xy} have been explained by the interband transitions due to the skyrmion scattering. The mass ratio dependence also affects the absolute value of the resistivity and does not substantially change the shape of the ρ_{xy}-curves. The direct and the topological Hall resistivities monotonically grow with temperature. There is still the mass ratio dependence for ρ_{xx}, ρ_{zz} and ρ_{xy}. Because the absolute value of $|\rho_{xy}| \ll |\rho_{zz} - \rho_{xx}|$, it could be difficult to identify ρ_{xy} that arises from the electron-skyrmion scattering. In real

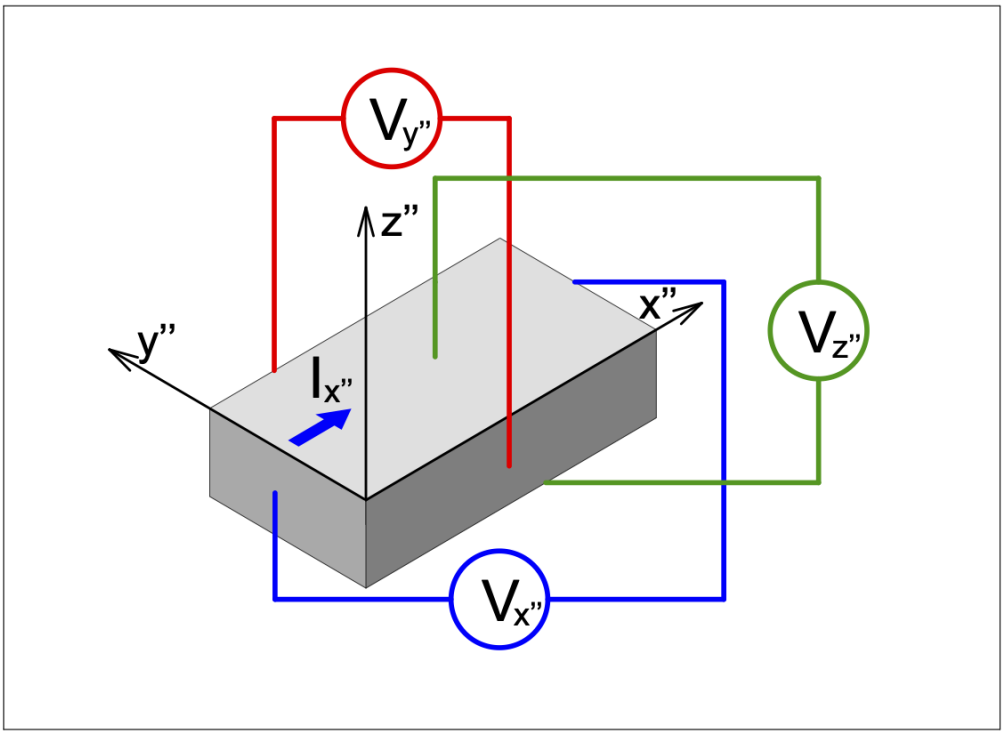

FIG. 8. Experimental setup, which allows for the measurements .of all three current components.

experiments, there can be a nonzero angle between the electric current and the crystal x-axis. In this case, the voltage is given by expression (15) where there is the term proportional to $|\rho_{zz} - \rho_{xx}|$, which dominates over the topological Hall contribution. Thus, we propose the experimental setup where the voltage has to be measured in all three directions. Knowing $V_{x''}$, $V_{y''}$, and $V_{z''}$ and the angles between the crystal axes and the electric current, ρ_{xy} can be identified using Eqs. (15).

ACKNOWLEDGMENT

This work was supported by a grants from the US National Science Foundation (No. 2228841) to the University of Wyoming.

REFERENCES

* yurid@uwyo.edu

[1] A. Bogdanov and D. Yablonskiui, Sov. Phys. JETP **68**, 101 (1989).

[2] U. K. Rößler, A. N. Bogdanov, and C. Pfleiderer, Nature **442**, 797 (2006).

[3] S. Mühlbauer, B. Binz, F. Jonietz, C. Pfleiderer, A. Rosch, A. Neubauer, R. Georgii, and P. Böni, Science **323**, 915 (2009).

[4] X. Z. Yu, Y. Onose, N. Kanazawa, J. H. Park, J. H. Han, Y. Matsui, N. Nagaosa, and Y. Tokura, Nature **465**, 901 (2010).

[5] X. Z. Yu, N. Kanazawa, Y. Onose, K. Kimoto, W. Z. Zhang, S. Ishiwata, Y. Matsui, and Y. Tokura, Nature Materials **10**, 106 (2011).

[6] S. Seki, X. Z. Yu, S. Ishiwata, and Y. Tokura, Science **336**, 198 (2012).

[7] T. Adams, A. Chacon, M. Wagner, A. Bauer, G. Brandl, B. Pedersen, H. Berger, P. Lemmens, and C. Pfleiderer, Phys. Rev. Lett. **108**, 237204 (2012).

[8] T. Kurumaji, T. Nakajima, M. Hirschberger, A. Kikkawa, Y. Yamasaki, H. Sagayama, H. Nakao, Y. Taguchi, T. hisa Arima, and Y. Tokura, Science **365**, 914 (2019).

[9] R. Yambe and S. Hayami, Scientific Reports **11**, 11184 (2021).

[10] M. Hirschberger, T. Nakajima, S. Gao, L. Peng, A. Kikkawa, T. Kurumaji, M. Kriener, Y. Yamasaki, H. Sagayama, H. Nakao, et al., Nature Communications **10**, 5831 (2019).

[11] N. D. Khanh, T. Nakajima, X. Yu, S. Gao, K. Shibata, M. Hirschberger, Y. Yamasaki, H. Sagayama, H. Nakao, L. Peng, et al., Nature Nanotechnology **15**, 444 (2020).

[12] Y. Yasui, C. J. Butler, N. D. Khanh, S. Hayami, T. Nomoto, T. Hanaguri, Y. Motome, R. Arita, T.-h. Arima, Y. Tokura, et al., Nature Communications **11**, 5925 (2020).

[13] D. Chakrabartty, S. Jamaluddin, S. K. Manna, and A. K. Nayak, Communications Physics **5**, 189 (2022).

[14] R. Takagi, N. Matsuyama, V. Ukleev, L. Yu, J. S. White, S. Francoual, J. L. Mardegan, S. Hayami, H. Saito, K. Kaneko, et al., Nature Communications **13**, 1472 (2022).

[15] S. Hayami, Journal of Physics: Materials (2022).

[16] Z. Wang, Y. Su, S.-Z. Lin, and C. D. Batista, Phys. Rev. Lett. **124**, 207201 (2020).

[17] R. Ozawa, S. Hayami, and Y. Motome, Phys. Rev. Lett. **118**, 147205 (2017).

[18] S. Hayami, R. Ozawa, and Y. Motome, Phys. Rev. B **95**, 224424 (2017).

[19] S. Hayami and Y. Motome, Phys. Rev. B **103**, 024439 (2021).

[20] A. Anselm, *Introduction to Semiconductor Theory* (Mir, Moscow, 1981).

[21] N. Nagaosa and Y. Tokura, Nature Nanotechnology **8**, 899 (2013).

[22] A. Zadorozhnyi and Y. Dahnovsky, Journal of Physics: Condensed Matter **32** (2020).

[23] A. Zadorozhnyi and Y. Dahnovsky, Physical Review B **103** (2021).

[24] J. Bouaziz, H. Ishida, S. Lounis, and S. Blügel, Phys. Rev. Lett. **126**, 147203 (2021).

[25] T. Schulz, R. Ritz, A. Bauer, M. Halder, M. Wagner, C. Franz, C. Pfleiderer, K. Everschor, M. Garst, and A. Rosch, Nature Physics **8**, 301 (2012).

[26] D. Liang, J. P. DeGrave, M. J. Stolt, Y. Tokura, and S. Jin, Nature Communications **6**, 8217 (2015).

[27] T. Fujita, M. B. A. Jalil, S. G. Tan, and S. Murakami, Journal of Applied Physics **110**, 121301 (2011).

[28] N. Nagaosa and Y. Tokura, Physica Scripta **2012**, 014020 (2012).

[29] M. Lee, W. Kang, Y. Onose, Y. Tokura, and N. P. Ong, Phys. Rev. Lett. **102**, 186601 (2009).

[30] J. Iwasaki, M. Mochizuki, and N. Nagaosa, Nature Communications **4**, 1463 (2013).

[31] W. Jiang, X. Zhang, G. Yu, W. Zhang, X. Wang, M. Benjamin Jungfleisch, J. E. Pearson, X. Cheng, O. Heinonen, K. L. Wang, et al., Nature Physics **13**, 162 (2017).

[32] C. Reichhardt, D. Ray, and C. J. O. Reichhardt, Phys. Rev. Lett. **114**, 217202 (2015).

[33] C. Reichhardt, C. J. O. Reichhardt, and M. V. Milošević, Rev. Mod. Phys. **94**, 035005 (2022).

[34] N. Verma, Z. Addison, and M. Randeria, Science Advances **8**, eabq2765 (2022).

[35] K. Nakazawa and H. Kohno, Phys. Rev. B **99**, 174425 (2019).

[36] F. R. Lux, F. Freimuth, S. Blügel, and Y. Mokrousov, Phys. Rev. Lett. **124**, 096602 (2020).

[37] K. S. Denisov, I. V. Rozhansky, N. S. Averkiev, and E. Lähderanta, Phys. Rev. Lett. **117**, 027202 (2016).

[38] K. S. Denisov, I. V. Rozhansky, N. S. Averkiev, and E. Lähderanta, Phys. Rev. B **98**, 195439 (2018).

[39] J. R. Taylor, *Scattering Theory: The quantum Theory on Nonrelativistic Collisions* (Wiley, New York, 1972).

[40] A. Zadorozhnyi and Y. Dahnovsky, J. Phys. Chem. C **125**, 11035 (2021).

[41] S. S. Pershoguba, S. Nakosai, and A. V. Balatsky, Phys. Rev. B **94**, 064513 (2016).